Heliyon 6 (2020) e03440

Contents lists available at ScienceDirect

Heliyon

journal homepage: www.cell.com/heliyon

Research article

Classification of clear cell renal cell carcinoma based on *PKM* alternative splicing

Xiangyu Li [a], Beste Turanli [b], Kajetan Juszczak [a], Woonghee Kim [a], Muhammad Arif [a], Yusuke Sato [c,d], Seishi Ogawa [c,e], Hasan Turkez [f], Jens Nielsen [g], Jan Boren [h], Mathias Uhlen [a], Cheng Zhang [a,i,**], Adil Mardinoglu [a,j,*]

[a] *Science for Life Laboratory, KTH - Royal Institute of Technology, Stockholm, Sweden*
[b] *Department of Bioengineering, Istanbul Medeniyet University, Istanbul, Turkey*
[c] *Department of Pathology and Tumor Biology, Institute for the Advanced Study of Human Biology (WPI-ASHBi), Kyoto University, Kyoto, Japan*
[d] *Department of Urology, Graduate School of Medicine, The University of Tokyo, Tokyo, Japan*
[e] *Department of Medicine, Centre for Hematology and Regenerative Medicine, Karolinska Institute, Stockholm, Sweden*
[f] *Department of Molecular Biology and Genetics, Erzurum Technical University, Erzurum, 25240, Turkey*
[g] *Department of Biology and Biological Engineering, Chalmers University of Technology, Gothenburg, Sweden*
[h] *Department of Molecular and Clinical Medicine, University of Gothenburg, Sahlgrenska University Hospital, Gothenburg, Sweden*
[i] *School of Pharmaceutical Sciences, Zhengzhou University, Zhengzhou, PR China*
[j] *Centre for Host–Microbiome Interactions, Dental Institute, King's College London, London, SE1 9RT, United Kingdom*

ARTICLE INFO

Keywords:
Bioinformatics
Cancer research
Systems biology
PKM
Alternative splicing
Transcriptomics
Biomarker
Drug repositioning

ABSTRACT

Clear cell renal cell carcinoma (ccRCC) accounts for 70–80% of kidney cancer diagnoses and displays high molecular and histologic heterogeneity. Hence, it is necessary to reveal the underlying molecular mechanisms involved in progression of ccRCC to better stratify the patients and design effective treatment strategies. Here, we analyzed the survival outcome of ccRCC patients as a consequence of the differential expression of four transcript isoforms of the pyruvate kinase muscle type (*PKM*). We first extracted a classification biomarker consisting of eight gene pairs whose within-sample relative expression orderings (REOs) could be used to robustly classify the patients into two groups with distinct molecular characteristics and survival outcomes. Next, we validated our findings in a validation cohort and an independent Japanese ccRCC cohort. We finally performed drug repositioning analysis based on transcriptomic expression profiles of drug-perturbed cancer cell lines and proposed that paracetamol, nizatidine, dimethadione and conessine can be repurposed to treat the patients in one of the subtype of ccRCC whereas chenodeoxycholic acid, fenoterol and hexylcaine can be repurposed to treat the patients in the other subtype.

1. Introduction

Clear cell renal cell carcinoma (ccRCC) is the most common subtype among renal cancer (Motzer et al., 2017) and ccRCC shows high inter individual heterogeneity (Ricketts et al., 2018). Thus, it is difficult to predict survival outcomes of patients in clinical practice and design effective therapeutic strategies. Previous studies have already proposed strategies for stratification of ccRCC patients into subgroups based on different genetic and/or transcriptomic characteristics and prognoses of the patients (Brannon et al., 2010; Cancer Genome Atlas Research, 2013; Kosari et al., 2005; Takahashi et al., 2001). However, these studies failed to identify a clinically practical biomarker for classification of the patients at the personalized level or recommend targeted chemotherapy regimens for these patients.

Pyruvate kinase muscle type (*PKM*) is an enzyme that is involved in the final step of glycolysis and catalyzes the formation of ATP from ADP as phosphoenolpyruvate undergoes dephosphorylation to pyruvate. It is one of the key regulators of Warburg effect in tumors. Many studies have reported that different alternative splicing isoforms of *PKM* promote tumorigenesis (Christofk et al., 2008a; Clower et al., 2010; Yang et al., 2012), cell proliferation (Christofk et al., 2008b; Huang et al., 2017; Li et al., 2014; Lunt et al., 2015; Morita et al., 2018; Yang et al., 2011),

* Corresponding author.
** Corresponding author.
E-mail addresses: cheng.zhang@scilifelab.se (C. Zhang), adilm@scilifelab.se (A. Mardinoglu).

https://doi.org/10.1016/j.heliyon.2020.e03440
Received 27 November 2019; Received in revised form 7 February 2020; Accepted 14 February 2020

metastasis (Xie et al., 2019; Yang et al., 2014) and poor prognoses of patients (Ahmed et al., 2007; Uhlen et al., 2017) in different cancers. In a previous study, *PKM* isoform switch mediated by *PTBP1* was found in ccRCC (Jiang et al., 2017). Interestingly, we also found four different isoforms of *PKM* play a very important role in controlling metabolism of ccRCC (Li et al., 2019b). We have observed that the expression level of four protein-coding transcripts of *PKM*, including ENST00000335181, which is encoding PKM2 and the most studied isoform of *PKM*, as well as ENST00000561609, ENST00000389093 and ENST00000568883 are highly associated with patients' prognoses (Li et al., 2019b). Among them, high expression of ENST00000335181 and ENST00000561609 indicated a favorable survival while high expression of ENST00000389093 and ENST00000568883 indicated an unfavorable survival. Moreover, a number of conserved biological functions associated with the progression of ccRCC were oppositely dysregulated by these transcripts. Here, we hypothesized that different molecular subtypes among ccRCC patients can be characterized by the different expression patterns induced by these four prognostic transcripts and biomarkers that may be used in clinical practice can be identified.

Systems biology based approaches have been used in stratification of patients with different metabolic diseases and certain type of cancers for characterization of the patient subtypes (Altay et al., 2019; Benfeitas et al., 2019; Bidkhori et al., 2018; Bjornson et al., 2015; Mardinoglu et al., 2018). Previous studies have also proposed transcriptomics-based biomarkers for classification of tumors based on the quantitative measurement of one or multiple signature genes (Fujita et al., 2012; Jones et al., 2005; Klatte et al., 2009; Kosari et al., 2005; Zhao et al., 2006). However, this kind of transcriptional signatures are rarely used in clinical practice due to technological and translational barriers (Winslow et al., 2012). Besides problems in tissue sampling and quality control, an important factor is experimental batch effect which brings high variation of gene expression induced by the different laboratory conditions and personnel (Guan et al., 2018). To solve these problems, the use of biomarkers based on the within-sample relative expression orderings (REOs) of gene pairs has been proposed (Guo et al., 2018; Qi et al., 2016a, 2016b). REOs-based biomarkers are robust against batch effects, invariant to monotone data normalization (Eddy et al., 2010; Wang et al., 2013) and poor sample preparation (Chen et al., 2017b; Cheng et al., 2017; Liu et al., 2017).

In this study, we used the genes dysregulated by the prognostic transcripts of *PKM* to extract classification biomarker instead of using themselves. Since different transcripts of *PKM* share similar sequence, it may be difficult to design distinct primers to detect their relative abundance when using real-time PCR. Thus, gene pair biomarker is more feasible and practical in clinical diagnosis. We applied REOs-based method to identify biomarkers for classification of ccRCC by extracting the expression profiles of genes which were consistently negatively dysregulated by the four favorable and unfavorable prognostic transcripts of *PKM*. We developed a REOs-based biomarker using the global gene expression profiling of ccRCC in The Cancer Genome Atlas (TCGA) database and stratified the patients into two subtypes exhibiting different transcriptomic expression patterns and different patient prognosis. We also validated our findings in TCGA database as well as in another independent Japanese cohort. We finally proposed several candidate drugs that can be used in treatment of each subtype based on transcriptomic expression profiles of drug-perturbed cancer cell lines from Connectivity Map 2.0 (CMap2).

2. Result

2.1. Identification of signature gene set associated with four prognostic transcripts of PKM

In a recent study, we have found that there are molecular subtypes that could be characterized by the expression of the four different prognostic *PKM* transcripts (Li et al., 2019b). In order to develop a REOs-based biomarker, we identified a signature gene set associated with these four transcripts based on the gene expression profiles of TCGA ccRCC samples. We performed differential expression analysis between the tumor samples from patients with high (top 25%) and low (bottom 25%) expression of each favorable transcript, and identified 2,010 consistently significantly (FDR <1.0e-5) differentially expressed genes (DEGs) for the two favorable transcripts (Figure 1). Similarly, we identified 5,469 DEGs consistently significantly (FDR <1.0e-5) DEGs for the two unfavorable transcripts. We found that the two sets of DEGs has a significant overlap (n = 1,135; hypergeometric distribution test, p < 1.11e-16). We also observed that the concordance score of these overlapped genes is 100%, which means the up-regulated genes associated with high expression of favorable transcripts within these 1,135 genes are all down-regulated when the unfavorable transcripts exhibit high expression; and vice versa.

We followed-up survival information from the corresponding patients and found that 539 of the 1,135 genes (of which 305 and 234 are favorable and unfavorable, respectively) are significantly (univariate Cox model, FDR <0.01) associated with patients' overall survival (OS). To identify the associated biological functions with these 539 genes, we performed GO term enrichment analysis and observed that these genes are significantly enriched in RNA splicing, RNA catabolic process and nuclear transport pathways (FDR<0.05; Table S1). Therefore, we concluded that these 539 genes may be used as the core signature genes that are associated with the differential alternative splicing of *PKM* among ccRCC patients and may be used for classification of tumor samples.

We calculated the co-expression coefficients between the expression of the 539 signature genes and found two major clusters in which all favorable genes are positively co-expressed while all unfavorable genes are negatively co-expressed in the opposite cluster using the hierarchical clustering (Figure 2A). Based on the expression profiles of these 539 signature genes, we employed consensus clustering to classify TCGA ccRCC samples into distinct stable sub-groups through repeated subsampling and clustering (Wilkerson and Hayes, 2010). As shown in Figure 2B, we determined an optimum number of two clusters, cluster 1 and 2, based on the lowest proportion of ambiguous clustering (Senbabaoglu et al., 2014). Using survival analysis, we observed the patients whose tumor samples classified in cluster 1 (N = 231) had significantly shorter OS than those classified in cluster 2 (N = 297) with statistical significance (log-rank test, P = 6.73e-07; Figure 2C). The results demonstrated that there are two different molecular subtypes in ccRCC with significantly different survival outcomes which are strongly associated with the function of the two favorable and two unfavorable transcripts.

2.2. Development of the REOs-based classification biomarker

To identify a biomarker that can be used in the clinical practice, we next focused on development of a REOs-based classification biomarker based on the gene expression profiles of the 539 signature genes. In brief, REOs-based biomarkers employs gene pairs with consistently reversed expression orders between the two molecular groups as indicators, and screens for a minimum combination of these gene pairs that serves as risk indicators for classification. In order to obtain a robust biomarker, we generated 100 training and 100 validation datasets by randomly selecting from TCGA ccRCC cohort and randomly separated the samples into two respective groups with 70% and 30% samples. We identified 171 gene pairs that exhibited consistent reverse gene pairs in all training datasets. We next generated 17,100 reverse gene pair combinations with a forward selection procedure and selected a final REOs-based biomarker consisted of eight reverse gene pairs with an optimal mean F-score of 0.9725 in all training datasets (Figure 2D). The full screening process are shown in Figure 1 and detailed in Method section.

Within this eight gene pairs, if more than four gene pairs exhibited reversal REOs in a sample, this sample would be classified into the high-

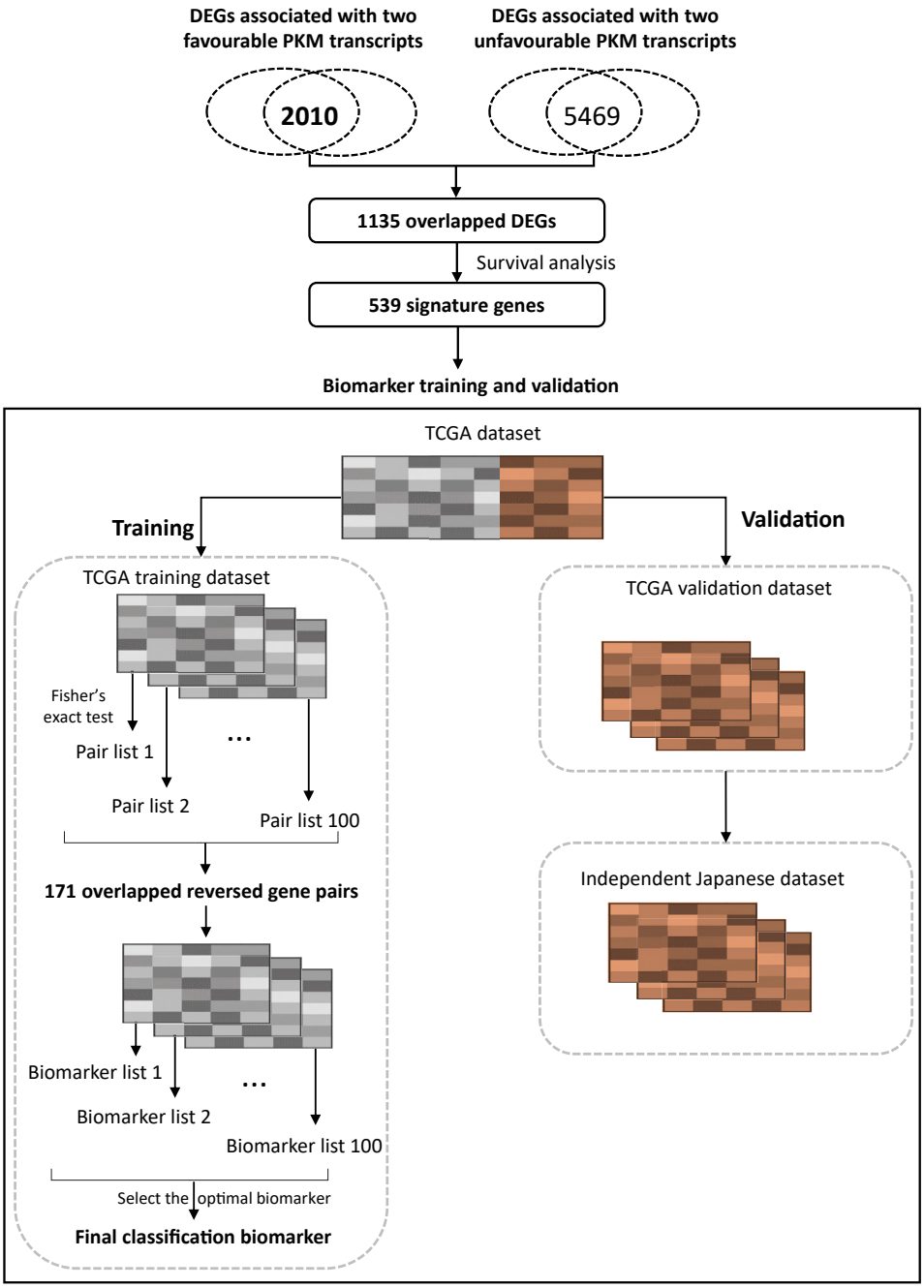

Figure 1. The flowchart for developing and validating the ccRCC classification biomarker. In brief, we extract the 1135 overlapped DEGs associated with favorable and unfavorable transcripts, and select 539 prognostic signature genes from them. Next, we screen gene pair biomarker using randomly generated training dataset. Lastly, we validate the performance of the biomarker in all randomly generated validation dataset and an independent Japanese ccRCC dataset.

risk group; otherwise, this sample would be classified into the low-risk group (Figure 2D). We tested these gene pairs in the 100 validation datasets, and found that these gene pairs also showed a good classification accuracy with a mean F-score 0.9742. We also tested these gene pairs using the complete TCGA cohort, and this biomarker classified 231 samples into high-risk group and 297 samples into low-risk group. Notably, these two groups showed significantly different OS (Figure 2E; log rank test, P = 1.69e-07).

2.3. Validation of the REOs-based classification biomarker

To validate if these gene pairs can be used as a biomarker for classification of ccRCC samples, we tested these gene pairs in 100 ccRCC samples obtained from an independent Japanese cohort. The biomarker classified 35 samples as high-risk group and 65 samples as low-risk group, and these two groups showed significantly different OS (Figure 2F, P = 7.46e-05). We next investigated whether the high and low-risk groups identified in both TCGA and Japanese cohorts exhibited similar biological differences. We extracted the top 20% most significant DEGs (n = 2,694) between high and low-risk groups in both the TCGA and Japanese cohorts, and observed a significant overlap between them (n = 1,463; hypergeometric distribution test, p < 1.11e-16) with a concordance score 100%. In addition, we identified 66 and 80 GO terms that are significantly enriched with upregulated genes (FDR<1.0e-05) in the high-risk group of the TCGA and Japanese cohorts, respectively, and found that 55 of them are common in both cohorts (Figure 3).

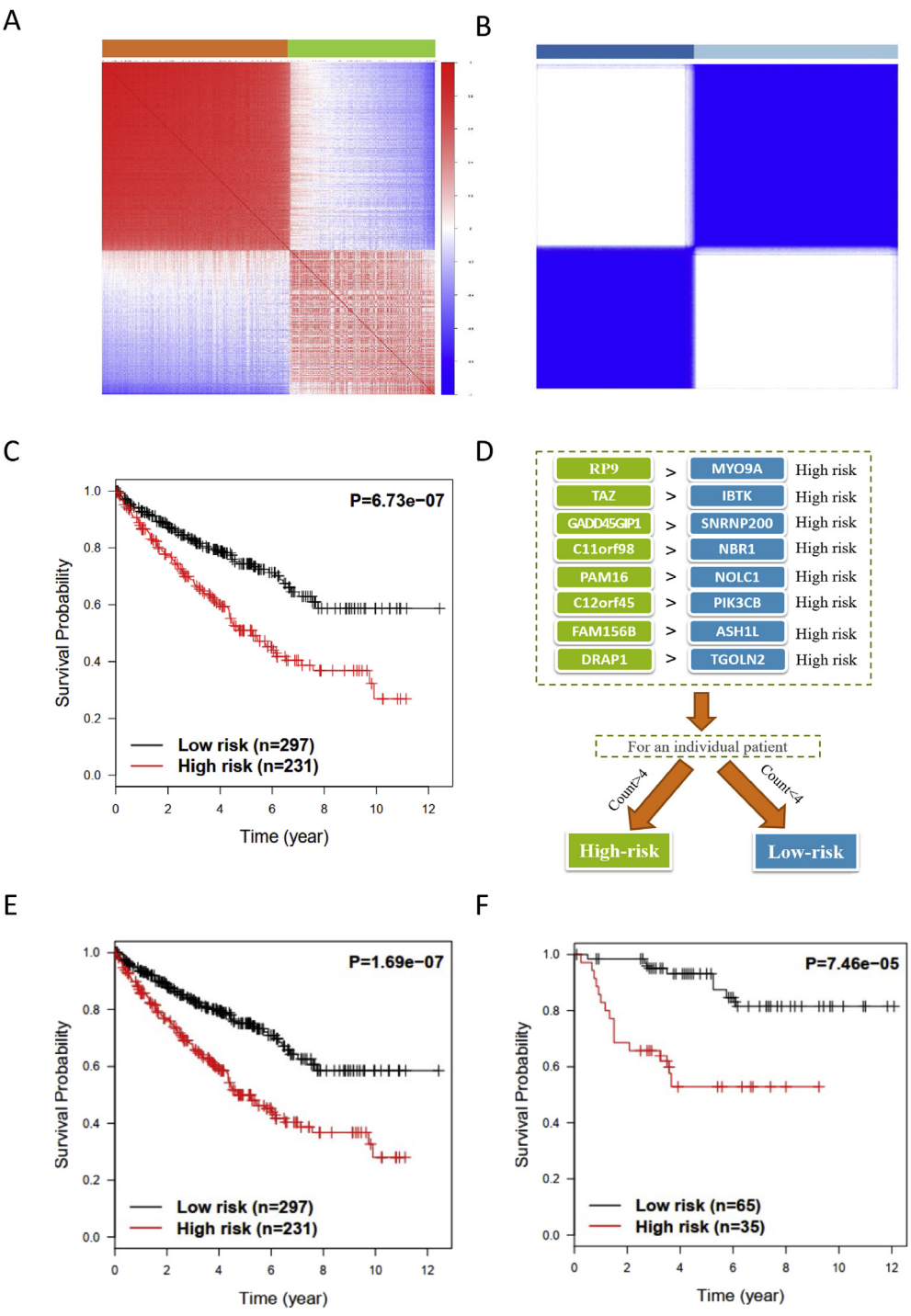

Figure 2. Molecular classification and prognostic prediction of patients by classification biomarker. (A) Hierarchical clustering of 539 signature genes based on the correlation between genes. The spearman correlation coefficients between genes were used for clustering. (B) Consensus clustering for TCGA ccRCC patients based on the expression values of the 539 signature genes. (C) Kaplan-Meier plot of OS of two clusters identified by consensus clustering in TCGA ccRCC cohort. (D) The composition of classification biomarker and voting rule. (E) Kaplan-Meier plot of OS of high- and low-risk identified by classification biomarker in TCGA ccRCC cohort. (F) Kaplan-Meier plot of OS of high- and low-risk identified by classification biomarker in Japanese ccRCC cohort.

Specifically, the high-risk group was characterized by upregulated genes involved in ATP synthesis, mitochondrial respiratory process, oxidative phosphorylation, ribonucleotide and purine nucleotide metabolic process, RNA catabolic process, protein targeting to ER and membrane pathways. And the low-risk group was characterized by upregulated genes involved in histone modification and covalent chromatin modification pathways. The results suggested the molecular subtypes identified by our analysis also have consistent biological differences. Moreover, these 55 GO terms included all 27 GO terms that we recently reported to be associated with the four different prognostic transcripts in pan cancer analysis (Li et al., 2019b). We also identified three GO terms that are significantly enriched with downregulated genes in the high-risk group for both cohorts, and two of them, which are the histone modification and covalent chromatin modification pathways, are common in both groups. These results further indicated that the molecular subtypes stratified by the gene pairs are functionally related to the four prognostic transcripts of *PKM*.

Further, we compared our REOs-based classification with previously reported TCGA (m1 to m4) and ccA/ccB classification schemes (Brannon et al., 2010; Cancer Genome Atlas Research, 2013) (Figure 4). In TCGA cohort, approximately 96% of TCGA m1 tumors were involved in our low-risk group, and m1 group was also reported with the best prognoses in TCGA classification scheme. In addition, 73% of TCGA tumors in both m2 and m4 subtypes were involved in our high-risk groups, and they

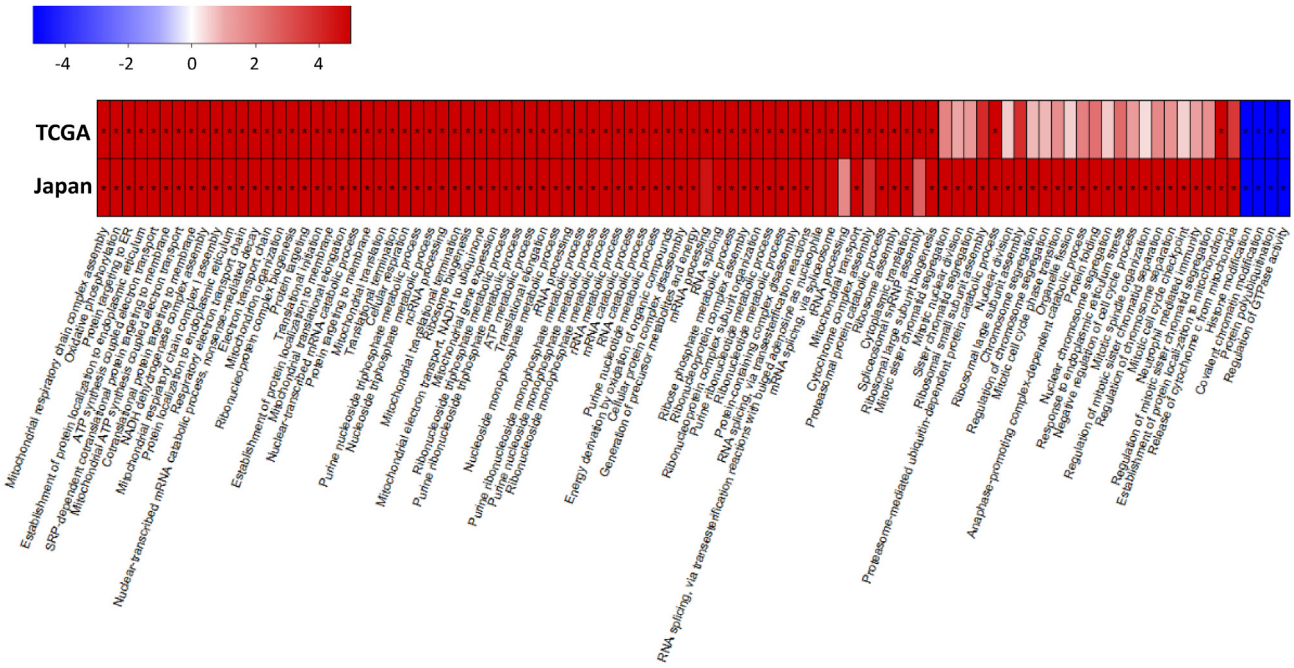

Figure 3. The dysregulated biological functions in high- and low-risk ccRCC groups and. Heat map of the p values (on the negative log 10 scale) for the enriched GO terms in TCGA and Japanese KIRC cohort. Red color denotes the GO terms enriched with up-regulated genes. Blue color denotes the GO terms enriched with down-regulated genes. * FDR<1.0e-05.

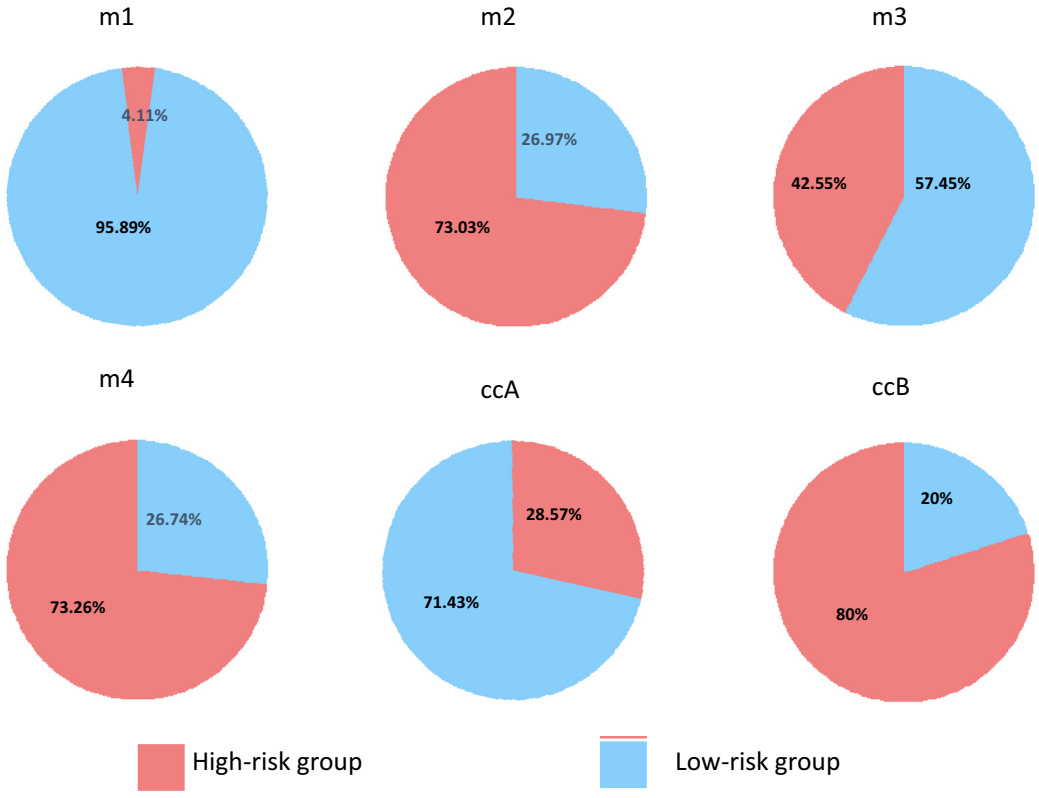

Figure 4. Pie charts showing the intersection of the different classification schemes for ccRCC. 'm1', 'm2', 'm3' and 'm4' indicate the molecular subtypes proposed by TCGA, and 'ccA' and 'ccB' are molecular subtypes reported by another previous study.

were also shown to be with the poorest prognoses in TCGA classification. These results demonstrated that the high and low-risk groups classified by our biomarker are reinforced by the previously observed survival outcomes m1, m2 and m4. Notably, the high and low-risk groups respectively accounted for 42% and 58% of tumors previously reported as unclassified (m3) in the TCGA classification scheme. In Japanese cohort, 71% of ccA and 80% of ccB were observed in the low and high-risk groups, respectively. We found that the favorable survival for

ccA cases again reinforced the low-risk group classification based on our gene pairs used as a biomarker (Figure 4).

2.4. Drug repositioning for treatment of ccRCC subtypes

In addition to classification of the tumors, we also performed drug repositioning analysis to identify drug candidates that can be used in treatment of each subtype (Figure 5). We assumed that if a drug could reverse the dysregulated gene expression pattern from a tumor subtype to normal pattern, it could be potentially useful for treating the specific tumor subtype. We used a method developed in our previous study for drug repurposing (Turanli et al., 2018, 2019a, 2019b) and found several drugs that could be used for treatment of the high and low-risk groups (see Method). We found that four different drugs including paracetamol, nizatidine, dimethadione and conessine may be used to reverse the gene expression in samples from high-risk group, since over 80% drug-perturbed genes were mapped to the DEGs between these samples and normal samples. Paracetamol is an analgesic and antipyretic drug with the effect of anti-inflammatory and inhibits the production of multiple oxidants (Graham et al., 2013). Interestingly, it has been reported that paracetamol inhibits the cell proliferation and induces cell apoptosis in pancreatic cancer (Malsy et al., 2017), ovarian cancer and lung cancer cells (Lian et al., 2018). Nizatidine is an antagonist of histamine H_2 receptors and these receptors are associated with cell proliferation, embryonic development and tumor growth (Fernandez-Nogueira et al., 2018). It has been shown that nizatidine was recommended to be added into the combination therapy for cancer treatment (Barton-Burke, 1996; Ben-Sasson, 2007; Feitelberg et al.,

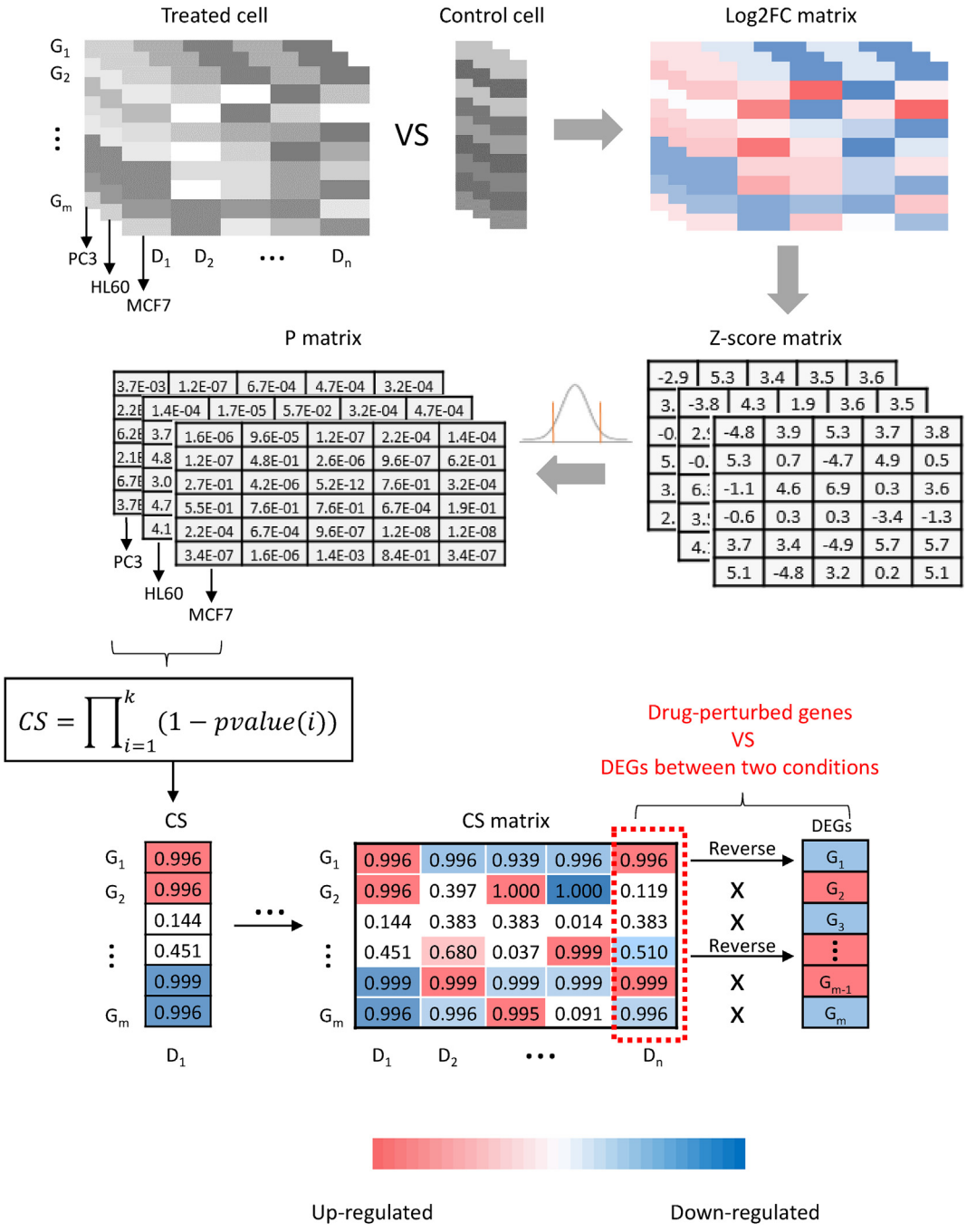

Figure 5. The flowchart for drug repositioning.

2013). Conessine, a steroid alkaloid, decreases basal NF-κB activity, regulates autophagy, has anti-inflammatory effect (Kim et al., 2016, 2018) and is proposed as a potential anti-cancer drug. Therefore, the anti-cancer effects of three of the proposed drugs have been reported in previous studies.

Similarly, we found that three different drugs including chenodeoxycholic acid, fenoterol and hexylcaine, may be used to reverse the gene expression in samples of low-risk group towards normal samples. It has been reported that natural as well as synthetic bile acids can modulate cell cycle and induce apoptosis in cancer cells (Horowitz et al., 2007; Kim et al., 2006). Chenodeoxycholic acid, a bile acid, shows anti-proliferative activity in human cancer cells (Faustino et al., 2016). Beta-adrenergic signaling pathway has been found to promote the initiation and progression of cancer including inflammation, angiogenesis, apoptosis, cell motility, DNA damage repair and epithelial-mesenchymal transition (Cole and Sood, 2012). Fenoterol, a beta-adrenoreceptor agonist, has been shown to inhibit the proliferation of glioblastomas and astrocytomas cells (Bernier et al., 2013; Toll et al., 2011). Hexylcaine, a short-acting local anesthetic, has also been used to treat cancer (Gleich, 2000) even its anti-cancer activity is still unclear. In this context, these three drugs may also be potentially used for treatment of the subtype of ccRCC patients.

Moreover, we identified the gene targets for each of the drugs using DrugBank database (Wishart et al., 2006). *HRH2*, encoding the histamine H_2 receptor, has been reported as the gene target of nizatidine (Meredith et al., 1985). We observed that it is significantly up-regulated in the samples of high-risk group compared to normal samples. It has been demonstrated that in vitro and in vivo histamine-induced tumor cell proliferation can be blocked by H_2 antagonists (Deva and Jameson, 2012; Natori et al., 2005; Tomita et al., 2003). Thus, nizatidine may be used as a promising drug for the patients classified in the high-risk group. On the other hand, *GPBAR1*, encoding an enzyme of the G protein-coupled receptor superfamily, has been reported as a target of chenodeoxycholic acid. It has been shown that *GPBAR1* antagonizes kidney cancer cell proliferation and migration (Su et al., 2017). Based on our analysis, we have observed that *GPBAR1* is significantly downregulated in the low-risk group compared to normal samples. Thus, chenodeoxycholic acid, as an activator of *GPBAR1*, may be used as a promising drug for treating the patients classified in the low-risk group.

3. Discussion

PKM is one of the important regulators of Warburg effect in different human cancers (Dayton et al., 2016). Our recent study showed that four different transcripts of *PKM* mediate opposite survival outcomes for ccRCC patients. In this study, we identified the core signature genes which were consistently dysregulated by these four prognostic transcripts of *PKM*. Using these signature genes, we identified eight gene pairs whose within-samples REOs could be used to classify patients into two groups with significantly different OS. Although RNA sequencing data was used for the biomarker classification in this study, much cheaper technics could be used once the biomarker is used in clinical practice. For instance, we could use real-time PCR, which is much cheaper compared to the sequencing approach, to determine the relative abundance of the genes involved in these 8 gene pairs to classify a ccRCC tumor sample since we only need to detect their REOs.

Real-time PCR has been used for commercial mRNA-based gene signatures. One FDA-approved signature is AlloMap®, consisting of 20 genes, for estimating the risk of acute cellular rejection in heart transplant recipients (Starling et al., 2006). Another FDA-approved signature is Oncotype DX®, consisting 21 genes, for estimating the risk of distant recurrence in tamoxifen-treated patients with node-negative, estrogen-receptor-positive breast cancer (Paik et al., 2004). Both of the signatures used in classification of patients into different risk groups by comparing their risk scores summarized from expression levels of the signature genes with preset risk score thresholds. However, the preset thresholds from the training dataset cannot be directly applied to independent dataset since the gene expression levels are sensitive to batch effects and platform differences (Qi et al., 2016a). To solve this problem, the tissue samples must be sent to the specified laboratories for measurement with uniform quality control and data normalization, which brings great limitations for wide application of these signatures. In contrast, the relative abundance of two genes in a gene pair is much easier to be estimated by real-time PCR with appropriate performance since REOs-based biomarkers are relatively insensitive to both experimental and bioinformatics variations, which could greatly facilitate the use of REOs-based biomarker in clinical practice.

The genes involved in our classification of ccRCC tumor samples also showed closed relationship with tumor development. For instance, *RP9*, one of genes in the REOs gene pairs, plays an important role in pre-mRNA splicing and could interact with well-known oncogene *PIM-1* (Maita et al., 2000). *MYO9A*, encodes an unconventional myosin, which is required for collective migration of epithelial cells and thus serves as a potent promoter in progression and metastasis of cancers of epithelial origin (Friedl and Gilmour, 2009; Ouderkirk and Krendel, 2014). *TAZ* encodes tafazzin whose overexpression promotes tumorigenicity in many cancers and its inhibition also induces tumor cell apoptosis (Chen et al., 2017a; Li et al., 2019a; Pathak et al., 2014). *GADD45GIP1*, also known as *CRIF1*, encodes a nuclear-localized protein that may be induced by *TP53* and regulates cell cycle. *CRIF1* is a novel transcriptional coactivator of *STAT3* which is a well-known oncogene in multiple human cancers (Kwon et al., 2008). However, *CRIF1* was recruited to the upstream promoter region of *TP53* to suppress cell cycle progression in HCT116 cells (Yan et al., 2017). Thus, the role of *CRIF1* is controversial in cancer. *SNRNP200* encodes a component of U5 snRNP-specific proteins of spliceosome. It has been shown that overexpression of *SNRNP200* was associated with tumor aggressiveness in prostate cancer (Jimenez-Vacas et al., 2020). *PIK3CB* is involved in the PI3K signaling pathway which is frequently dysregulated in cancer. Inhibition of *PIK3CB* remarkably suppressed cell growth, migration and enhanced apoptosis in glioblastoma (Cen et al., 2018; Pridham et al., 2018). *NOLC1* functions as a chaperone for shuttling between the nucleolus and cytoplasm (Meier and Blobel, 1992). It has been reported that enhancement of *NOLC1* promotes cell senescence and represses hepatocellular carcinoma cell proliferation by disturbing the organization of nucleolus (Yuan et al., 2017).

The immunotherapy is widely used in ccRCC since the disturbance of different immunological pathways were observed in ccRCC (Lopez-Beltran et al., 2018). In this study, we found some of our biomarker genes are potential targets for immunotherapy. *TAZ* also acts as a regulator in immune evasion of cancer by positively modulating the expression of *PD-L1* in mRNA and protein level (Janse van Rensburg et al., 2018), which is a potential maker for immunotherapy. In our analysis, both *TAZ* and *PD-L1* are significantly highly expressed in high- or low-risk samples compared with normal samples. Especially, the expression of *TAZ* is much higher in high-risk patients than low-risk patients, suggesting that targeting *TAZ* is a more promising treatment strategy for high-risk patients besides *PD-L1* immunotherapy. *MYO9A* is highly expressed in immune cells and plays an important role in regulation of macrophage shape and motility (Bahler et al., 2011). In our analysis, *MYO9A* was significantly down-regulated in high-risk samples compared with low-risk and normal samples, suggesting the innate immune response may be weak in high-risk ccRCC patients. *IBTK* encodes the inhibitor of Bruton tyrosine kinase which is required for B cell survival, differentiation and activation (Fiume et al., 2009). In our analysis, the expression of *IBTK* was increasingly down-regulated in normal, low-risk and high-risk samples, suggesting that B cell immune system is active in ccRCC. *NBR1* encodes a specific autophagy receptor. It has been reported that NBR1-deficient mice have defective T helper 2 cell differentiation (Yang et al., 2010). The histone methyltransferase *ASH1L* is involved in the regulation of regulatory T cell polarization (Xia et al., 2017). In our analysis, both the expression of *NBR1* and *ASH1L* were increasingly down-regulated in normal, low-risk and high-risk samples, suggesting

that T cell immune system may be impaired in ccRCC. *PIK3CB* is critical in neutrophil activation by immune complexes (Kulkarni et al., 2011), which is significantly down-regulated in the high-risk samples compared to low-risk and normal samples.

In conclusion, we identified two molecular subtypes of ccRCC patients with high and low-risk of mortality, and developed a REOs-based classification biomarker which could be used to classify the ccRCC patients into these subtypes at personalized level. In addition, we suggested specific treatment strategies for each subtype based on their global gene expression patterns and drug repositioning. Therefore, it is worthwhile to further explore the potential clinical use of the here identified biomarker in assisting clinical diagnosis and treatment of ccRCC patients.

4. Materials and methods

4.1. Data and preprocessing

The TCGA transcript-expression level profiles (TPM and count values) of ccRCC and matched normal kidney samples was downloaded from https://osf.io/gqrz9 (Tatlow and Piccolo, 2016) on November 27, 2018, which was quantified by Kallisto (Bray et al., 2016) based on the GENCODE reference transcriptome (version 24). The clinical information of TCGA samples was downloaded through R package TCGAbiolinks (Colaprico et al., 2016). The whole-exome sequence data of 100 ccRCC samples of patients from Japanese cohort (Sato et al., 2013) was downloaded from European Genome-phenome Archive (accession number: EGAS00001000509). BEDTools (Quinlan and Hall, 2010) was used for converting BAM to FASTQ file. Kallisto was used for estimating the count and TPM values of transcripts based on the same reference transcriptome of TCGA data. The sum value of the multiple transcripts of a gene was used as the expression value of this gene. The genes with average TPM values > 1 in ccRCC patients were analyzed.

4.2. Differential expression analysis

DESeq2 (Love et al., 2014) was used to identify DEGs between two groups. The raw count values of genes were used as input of DESeq2. The Benjamini-Hochberg (BH) procedure was used to estimate FDR.

4.3. Overlapping of two lists of DEGs

If DEG list 1 with L_1 genes and DEG list 2 with L_2 genes have k overlapping genes and s of these genes shows the same directions which means high expression of these genes indicates favorable/unfavorable survival or group 1/2 in both lists, the probability of observing at least s consistent genes by chance can be calculated according to the following cumulative hypergeometric distribution model:

$$P = 1 - \sum_{i=0}^{s-1} \frac{\binom{L2}{i}\binom{L-L2}{L1-i}}{\binom{L}{L1}} \quad (1)$$

where L represents the number of the background genes commonly detected in the datasets from which the DEGs are extracted. The two DEG lists were considered to be significantly overlapping if $P < 0.05$.

The concordance score s/k is used to evaluate the consistency of DEGs between the two lists. Obviously, the score ranges from 0 to 1, and the higher concordance score suggests the better consistency of two lists of DEGs.

4.4. Consensus clustering

Consensus clustering (Wilkerson and Hayes, 2010) was used for tumor classification based on the normalized expression profiles of signature genes by Z-score transformation. To achieve robust clusters, the data was resampled for 1000 times by considering 80% samples and signature genes resampling. The resampled data was transformed into a similarity matrix, termed as consensus matrix. K-means clustering was used to stratify samples based on the consensus matrix. The number of optimum cluster was determined by the lowest proportion of ambiguous clustering.

4.5. Survival analysis

The univariate Cox regression model was used to evaluate the correlation of gene expression levels with OS. Survival curves were estimated by the Kaplan-Meier method and compared with the log-rank test.

4.6. Functional enrichment analysis

GO enrichment was performed by the enrichGo function in R package ClusterProfiler (Yu et al., 2012), in which the hypergeometric distribution was used to calculate the statistical significance of biological pathways enriched with DEGs of interest.

4.7. Development of the REOs-based biomarker

In each sample, the REO of every two signature genes (i and j) is denoted as either $G_i > G_j$ or $G_i < G_j$ exclusively, where G_i and G_j represent the expression values of gene i and j, respectively. For a given gene pair (G_i and G_j), we used Fisher's exact test to evaluate whether the frequency of group 1 samples with a specific REO pattern ($G_i > G_j$ or $G_i < G_j$) was significantly different from that in group 2 samples in each training dataset. The P values are adjusted using BH procedure. The gene pairs detected with 0.05 FDR control and over 70% difference of the frequency of their REOs between two groups were denoted as reversed gene pairs. The overlapped reversed gene pairs consistently identified from all the training datasets were selected as the candidate signature gene pairs. Totally, we found 171 signature gene pairs. For each signature gene pair, according to their within-sample REO, we classified the samples of each training dataset into high or low-risk groups and then evaluated the sensitivity and specificity of this gene pair. Here, the sensitivity is defined as the ratio of correctly identified high risk samples to all high-risk samples and the specificity is defined as the ratio of correctly identified low-risk samples to all low-risk samples. Then, from these signature gene pairs, we performed a forward selection procedure in each training dataset to search a set of gene pairs that achieved the highest F-score value, a harmonic mean of sensitivity and specificity, which is calculated as follows:

$$F - score = \frac{2(\text{sensitivity} * \text{specificity})}{(\text{sensitivity} + \text{specificity})} \quad (2)$$

Taking each of the 171 gene pairs as a seed, we added another gene pair to the biomarker at a time until the F-score did not increase. The classification rule is that a sample is classified into high or low-risk group if the majority of the REOs of the set of gene pairs within this sample vote for high or low-risk. We got 171 biomarkers based on each training dataset. Totally, we got 17,100 candidate biomarkers for all the 100 training datasets. Finally, we selected the biomarker with the lowest $(1\text{-}F_1)^2+(1\text{-}F_2)^2+\cdots+(1\text{-}F_n)^2$ as the final biomarker, in which F_n is the F-score value in the n^{th} training dataset.

4.8. Application of CMap2 data to drug discovery

The pre-procession of CMap2 data was described in our previous study (Turanli et al., 2019b). In brief, the gene expression profiles of three cell lines, HL60, MCF2 and PC3, were downloaded from https://portals. broadinstitute.org/cmap/(CMap Build 02). As shown in Figure 5, a single treatment cell line and control were selected to calculate Log2FC of genes by comparison between the two cases for each

cell line. We normalized the log2FC matrix with 12,228 genes and 683 drugs to z-score matrix and further transformed it to P value matrix. Then, the confidence score was calculated per each drug-gene interaction using the P values from three cell lines. An approximation confidence score to 1 was assumed as the higher confidence level. The drug-gene pairs with CS $>$ 0.5 were used in further analysis. If over 80% drug-perturbed genes with CS $>$ 0.5 were mapped to the DEGs between one subtype of cancer samples and normal samples, this drug is considered to have reverse effect on the dysregulated gene expression in this subtype of cancer samples.

Declarations

Author contribution statement

Xiangyu Li, Cheng Zhang, Adil Mardinoglu: Conceived and designed the analysis; Analyzed and interpreted the data; Wrote the paper.

Beste Turanli, Kajetan Juszczak, Woonghee Kim, Muhammad Arif, Yusuke Sato, Seishi Ogawa, Hasan Turkez, Jens Nielsen, Jan Boren, Mathias Uhlen: Contributed analysis tools or data; Wrote the paper.

Funding statement

This work was supported by The Knut and Alice Wallenberg Foundation.

Competing interest statement

The authors declare no conflict of interest.

Additional information

Supplementary content related to this article has been published online at https://doi.org/10.1016/j.heliyon.2020.e03440.

References

Ahmed, A.S., Dew, T., Lawton, F.G., Papadopoulos, A.J., Devaja, O., Raju, K.S., Sherwood, R.A., 2007. M2-PK as a novel marker in ovarian cancer. A prospective cohort study. Eur. J. Gynaecol. Oncol. 28, 83–88.

Altay, O., Nielsen, J., Uhlen, M., Boren, J., Mardinoglu, A., 2019. Systems biology perspective for studying the gut microbiota in human physiology and liver diseases. EBioMed. 49, 364–373.

Bahler, M., Elfrink, K., Hanley, P.J., Thelen, S., Xu, Y., 2011. Cellular functions of class IX myosins in epithelia and immune cells. Biochem. Soc. Trans. 39, 1166–1168.

Barton-Burke, M., 1996. Cancer Chemotherapy: A Nursing Process Approach. Jones & Bartlett Learning.

Ben-Sasson, S.A. (2007). Anti-cancer therapy comprising an H2-blocker, at least one antiinflammatory agent and a cytotoxic agent. United States patent US7838513B2.

Benfeitas, R., Bidkhori, G., Mukhopadhyay, B., Klevstig, M., Arif, M., Zhang, C., Lee, S., Cinar, R., Nielsen, J., Uhlen, M., et al., 2019. Characterization of heterogeneous redox responses in hepatocellular carcinoma patients using network analysis. EBioMed. 40, 471–487.

Bernier, M., Paul, R.K., Dossou, K.S., Wnorowski, A., Ramamoorthy, A., Paris, A., Moaddel, R., Cloix, J.F., Wainer, I.W., 2013. Antitumor activity of (R,R')-4-methoxy-1-naphthylfenoterol in a rat C6 glioma xenograft model in the mouse. Pharmacol. Res. Perspect. 1, e00010.

Bidkhori, G., Benfeitas, R., Klevstig, M., Zhang, C., Nielsen, J., Uhlen, M., Boren, J., Mardinoglu, A., 2018. Metabolic network-based stratification of hepatocellular carcinoma reveals three distinct tumor subtypes. Proc. Natl. Acad. Sci. U. S. A. 115, E11874–E11883.

Bjornson, E., Mukhopadhyay, B., Asplund, A., Pristovsek, N., Cinar, R., Romeo, S., Uhlen, M., Kunos, G., Nielsen, J., Mardinoglu, A., 2015. Stratification of hepatocellular carcinoma patients based on acetate utilization. Cell Rep. 13, 2014–2026.

Brannon, A.R., Reddy, A., Seiler, M., Arreola, A., Moore, D.T., Pruthi, R.S., Wallen, E.M., Nielsen, M.E., Liu, H., Nathanson, K.L., et al., 2010. Molecular stratification of clear cell renal cell carcinoma by consensus clustering reveals distinct subtypes and survival patterns. Genes Cancer 1, 152–163.

Bray, N.L., Pimentel, H., Melsted, P., Pachter, L., 2016. Near-optimal probabilistic RNA-seq quantification. Nat. Biotechnol. 34, 525–527.

Cancer Genome Atlas Research, N., 2013. Comprehensive molecular characterization of clear cell renal cell carcinoma. Nature 499, 43–49.

Cen, B., Wei, Y., Huang, W., Teng, M., He, S., Li, J., Wang, W., He, G., Bai, X., Liu, X., et al., 2018. An efficient bivalent cyclic RGD-PIK3CB siRNA conjugate for specific targeted therapy against glioblastoma in vitro and in vivo. Mol. Ther. Nucleic Acids 13, 220–232.

Chen, M., Zhang, Y., Zheng, P.S., 2017a. Tafazzin (TAZ) promotes the tumorigenicity of cervical cancer cells and inhibits apoptosis. PloS One 12, e0177171.

Chen, R., Guan, Q., Cheng, J., He, J., Liu, H., Cai, H., Hong, G., Zhang, J., Li, N., Ao, L., et al., 2017b. Robust transcriptional tumor signatures applicable to both formalin-fixed paraffin-embedded and fresh-frozen samples. Oncotarget 8, 6652–6662.

Cheng, J., Guo, Y., Gao, Q., Li, H., Yan, H., Li, M., Cai, H., Zheng, W., Li, X., Jiang, W., et al., 2017. Circumvent the uncertainty in the applications of transcriptional signatures to tumor tissues sampled from different tumor sites. Oncotarget 8, 30265–30275.

Christofk, H.R., Vander Heiden, M.G., Harris, M.H., Ramanathan, A., Gerszten, R.E., Wei, R., Fleming, M.D., Schreiber, S.L., Cantley, L.C., 2008a. The M2 splice isoform of pyruvate kinase is important for cancer metabolism and tumour growth. Nature 452, 230–233.

Christofk, H.R., Vander Heiden, M.G., Wu, N., Asara, J.M., Cantley, L.C., 2008b. Pyruvate kinase M2 is a phosphotyrosine-binding protein. Nature 452, 181–186.

Clower, C.V., Chatterjee, D., Wang, Z., Cantley, L.C., Vander Heiden, M.G., Krainer, A.R., 2010. The alternative splicing repressors hnRNP A1/A2 and PTB influence pyruvate kinase isoform expression and cell metabolism. Proc. Natl. Acad. Sci. U. S. A. 107, 1894–1899.

Colaprico, A., Silva, T.C., Olsen, C., Garofano, L., Cava, C., Garolini, D., Sabedot, T.S., Malta, T.M., Pagnotta, S.M., Castiglioni, I., et al., 2016. TCGAbiolinks: an R/Bioconductor package for integrative analysis of TCGA data. Nucleic Acids Res. 44, e71.

Cole, S.W., Sood, A.K., 2012. Molecular pathways: beta-adrenergic signaling in cancer. Clin. Canc. Res. 18, 1201–1206.

Dayton, T.L., Jacks, T., Vander Heiden, M.G., 2016. PKM2, cancer metabolism, and the road ahead. EMBO Rep. 17, 1721–1730.

Deva, S., Jameson, M., 2012. Histamine type 2 receptor antagonists as adjuvant treatment for resected colorectal cancer. Cochrane Database Syst. Rev., CD007814

Eddy, J.A., Sung, J., Geman, D., Price, N.D., 2010. Relative expression analysis for molecular cancer diagnosis and prognosis. Technol. Canc. Res. Treat. 9, 149–159.

Faustino, C., Serafim, C., Rijo, P., Reis, C.P., 2016. Bile acids and bile acid derivatives: use in drug delivery systems and as therapeutic agents. Expet Opin. Drug Deliv. 13, 1133–1148.

Feitelberg, D., Berkman, T., Ben-Sasson, S., and Goldstaub, D. (2013). Combination Therapy for the Treatment of Cancer. United States patent US20150005252A1.

Fernandez-Nogueira, P., Noguera-Castells, A., Fuster, G., Recalde-Percaz, L., Moragas, N., Lopez-Plana, A., Enreig, E., Jauregui, P., Carbo, N., Almendro, V., et al., 2018. Histamine receptor 1 inhibition enhances antitumor therapeutic responses through extracellular signal-regulated kinase (ERK) activation in breast cancer. Cancer Lett. 424, 70–83.

Fiume, G., Rossi, A., Di Salle, E., Spatuzza, C., Mallardo, M., Scala, G., Quinto, I., 2009. Computational analysis and in vivo validation of a microRNA encoded by the IBTK gene, a regulator of B-lymphocytes differentiation and survival. Comput. Biol. Chem. 33, 434–439.

Friedl, P., Gilmour, D., 2009. Collective cell migration in morphogenesis, regeneration and cancer. Nat. Rev. Mol. Cell Biol. 10, 445–457.

Fujita, T., Iwamura, M., Ishii, D., Tabata, K., Matsumoto, K., Yoshida, K., Baba, S., 2012. C-reactive protein as a prognostic marker for advanced renal cell carcinoma treated with sunitinib. Int. J. Urol. 19, 908–913.

Gleich, G.J. (2000). Topical Anesthetics Useful for Treating Cancer. United States patent US6391888B1.

Graham, G.G., Davies, M.J., Day, R.O., Mohamudally, A., Scott, K.F., 2013. The modern pharmacology of paracetamol: therapeutic actions, mechanism of action, metabolism, toxicity and recent pharmacological findings. Inflammopharmacology 21, 201–232.

Guan, Q., Yan, H., Chen, Y., Zheng, B., Cai, H., He, J., Song, K., Guo, Y., Ao, L., Liu, H., et al., 2018. Quantitative or qualitative transcriptional diagnostic signatures? A case study for colorectal cancer. BMC Genom. 19, 99.

Guo, Y., Jiang, W., Ao, L., Song, K., Chen, H., Guan, Q., Gao, Q., Cheng, J., Liu, H., Wang, X., et al., 2018. A qualitative signature for predicting pathological response to neoadjuvant chemoradiation in locally advanced rectal cancers. Radiother. Oncol. 129, 149–153.

Horowitz, N.S., Hua, J., Powell, M.A., Gibb, R.K., Mutch, D.G., Herzog, T.J., 2007. Novel cytotoxic agents from an unexpected source: bile acids and ovarian tumor apoptosis. Gynecol. Oncol. 107, 344–349.

Huang, J.Z., Chen, M., Chen, Gao, X.C., Zhu, S., Huang, H., Hu, M., Zhu, H., Yan, G.R., 2017. A peptide encoded by a putative lncRNA HOXB-AS3 suppresses colon cancer growth. Mol. Cell 68, 171–184 e176.

Janse van Rensburg, H.J., Azad, T., Ling, M., Hao, Y., Snetsinger, B., Khanal, P., Minassian, L.M., Graham, C.H., Rauh, M.J., Yang, X., 2018. The hippo pathway component TAZ promotes immune evasion in human cancer through PD-L1. Cancer Res. 78, 1457–1470.

Jiang, J., Chen, X., Liu, H., Shao, J., Xie, R., Gu, P., Duan, C., 2017. Polypyrimidine Tract-Binding Protein 1 promotes proliferation, migration and invasion in clear-cell renal cell carcinoma by regulating alternative splicing of PKM. Am. J. Cancer Res. 7, 245–259.

Jimenez-Vacas, J.M., Herrero-Aguayo, V., Montero-Hidalgo, A.J., Gomez-Gomez, E., Fuentes-Fayos, A.C., Leon-Gonzalez, A.J., Saez-Martinez, P., Alors-Perez, E., Pedraza-Arevalo, S., Gonzalez-Serrano, T., et al., 2020. Dysregulation of the splicing machinery is directly associated to aggressiveness of prostate cancer. EBioMed. 51, 102547.

Jones, J., Otu, H., Spentzos, D., Kolia, S., Inan, M., Beecken, W.D., Fellbaum, C., Gu, X., Joseph, M., Pantuck, A.J., et al., 2005. Gene signatures of progression and metastasis in renal cell cancer. Clin. Canc. Res. 11, 5730–5739.

Kim, H., Jang, M., Park, R., Jo, D., Choi, I., Choe, J., Oh, W.K., Park, J., 2018. Conessine treatment reduces dexamethasone-induced muscle atrophy by regulating MuRF1 and atrogin-1 expression. J. Microbiol. Biotechnol. 28, 520–526.

Kim, H., Lee, K.I., Jang, M., Namkoong, S., Park, R., Ju, H., Choi, I., Oh, W.K., Park, J., 2016. Conessine interferes with oxidative stress-induced C2C12 myoblast cell death through inhibition of autophagic flux. PloS One 11, e0157096.

Kim, N.D., Im, E., Yoo, Y.H., Choi, Y.H., 2006. Modulation of the cell cycle and induction of apoptosis in human cancer cells by synthetic bile acids. Curr. Cancer Drug Targets 6, 681–689.

Klatte, T., Seligson, D.B., LaRochelle, J., Shuch, B., Said, J.W., Riggs, S.B., Zomorodian, N., Kabbinavar, F.F., Pantuck, A.J., Belldegrun, A.S., 2009. Molecular signatures of localized clear cell renal cell carcinoma to predict disease-free survival after nephrectomy. Cancer Epidemiol. Biomark. Prev. 18, 894–900.

Kosari, F., Parker, A.S., Kube, D.M., Lohse, C.M., Leibovich, B.C., Blute, M.L., Cheville, J.C., Vasmatzis, G., 2005. Clear cell renal cell carcinoma: gene expression analyses identify a potential signature for tumor aggressiveness. Clin. Canc. Res. 11, 5128–5139.

Kulkarni, S., Sitaru, C., Jakus, Z., Anderson, K.E., Damoulakis, G., Davidson, K., Hirose, M., Juss, J., Oxley, D., Chessa, T.A., et al., 2011. PI3Kbeta plays a critical role in neutrophil activation by immune complexes. Sci. Signal. 4, ra23.

Kwon, M.C., Koo, B.K., Moon, J.S., Kim, Y.Y., Park, K.C., Kim, N.S., Kwon, M.Y., Kong, M.P., Yoon, K.J., Im, S.K., et al., 2008. Crif1 is a novel transcriptional coactivator of STAT3. EMBO J. 27, 642–653.

Li, L., Zhang, Y., Qiao, J., Yang, J.J., Liu, Z.R., 2014. Pyruvate kinase M2 in blood circulation facilitates tumor growth by promoting angiogenesis. J. Biol. Chem. 289, 25812–25821.

Li, X., Wu, M., An, D., Yuan, H., Li, Z., Song, Y., Liu, Z., 2019a. Suppression of Tafazzin promotes thyroid cancer apoptosis via activating the JNK signaling pathway and enhancing INF2-mediated mitochondrial fission. J. Cell. Physiol.

Li, X., Zhang, C., Kim, W., Arif, M., Gao, C., Hober, A., Kotol, D., Strandberg, L., Forsström1, B., Sivertsson, A., et al., 2019b. Discovery of Functional Alternatively Spliced PKM Transcripts in Human Cancers. bioRXIV. https://www.biorxiv.org/content/10.1101/613364v613361.

Lian, X., Huang, Y., Zhu, Y., Fang, Y., Zhao, R., Joseph, E., Li, J., Pellois, J.P., Zhou, H.C., 2018. Enzyme-MOF nanoreactor activates nontoxic paracetamol for cancer therapy. Angew Chem. Int. Ed. Engl. 57, 5725–5730.

Liu, H., Li, Y., He, J., Guan, Q., Chen, R., Yan, H., Zheng, W., Song, K., Cai, H., Guo, Y., et al., 2017. Robust transcriptional signatures for low-input RNA samples based on relative expression orderings. BMC Genom. 18, 913.

Lopez-Beltran, A., Henriques, V., Cimadamore, A., Santoni, M., Cheng, L., Gevaert, T., Blanca, A., Massari, F., Scarpelli, M., Montironi, R., 2018. The identification of immunological biomarkers in kidney cancers. Front. Oncol 8, 456.

Love, M.I., Huber, W., Anders, S., 2014. Moderated estimation of fold change and dispersion for RNA-seq data with DESeq2. Genome Biol. 15, 550.

Lunt, S.Y., Muralidhar, V., Hosios, A.M., Israelsen, W.J., Gui, D.Y., Newhouse, L., Ogrodzinski, M., Hecht, V., Xu, K., Acevedo, P.N., et al., 2015. Pyruvate kinase isoform expression alters nucleotide synthesis to impact cell proliferation. Mol. Cell 57, 95–107.

Maita, H., Harada, Y., Nagakubo, D., Kitaura, H., Ikeda, M., Tamai, K., Takahashi, K., Ariga, H., Iguchi-Ariga, S.M., 2000. PAP-1, a novel target protein of phosphorylation by pim-1 kinase. Eur. J. Biochem. 267, 5168–5178.

Malsy, M., Graf, B., Bundscherer, A., 2017. Effects of metamizole, MAA, and paracetamol on proliferation, apoptosis, and necrosis in the pancreatic cancer cell lines PaTu 8988 t and Panc-1. BMC Pharmacol. Toxicol. 18, 77.

Mardinoglu, A., Boren, J., Smith, U., Uhlen, M., Nielsen, J., 2018. Systems biology in hepatology: approaches and applications. Nat. Rev. Gastroenterol. Hepatol. 15, 365–377.

Meier, U.T., Blobel, G., 1992. Nopp140 shuttles on tracks between nucleolus and cytoplasm. Cell 70, 127–138.

Meredith, C.G., Speeg Jr., K.V., Schenker, S., 1985. Nizatidine, a new histamine H2-receptor antagonist, and hepatic oxidative drug metabolism in the rat: a comparison with structurally related compounds. Toxicol. Appl. Pharmacol. 77, 315–324.

Morita, M., Sato, T., Nomura, M., Sakamoto, Y., Inoue, Y., Tanaka, R., Ito, S., Kurosawa, K., Yamaguchi, K., Sugiura, Y., et al., 2018. PKM1 confers metabolic advantages and promotes cell-autonomous tumor cell growth. Canc. Cell 33, 355–367 e357.

Motzer, R.J., Jonasch, E., Agarwal, N., Bhayani, S., Bro, W.P., Chang, S.S., Choueiri, T.K., Costello, B.A., Derweesh, I.H., Fishman, M., et al., 2017. Kidney cancer, version 2.2017, NCCN clinical practice guidelines in oncology. J. Natl. Compr. Canc. Netw. 15, 804–834.

Natori, T., Sata, M., Nagai, R., Makuuchi, M., 2005. Cimetidine inhibits angiogenesis and suppresses tumor growth. Biomed. Pharmacother. 59, 56–60.

Ouderkirk, J.L., Krendel, M., 2014. Non-muscle myosins in tumor progression, cancer cell invasion, and metastasis. Cytoskeleton (Hoboken) 71, 447–463.

Paik, S., Shak, S., Tang, G., Kim, C., Baker, J., Cronin, M., Baehner, F.L., Walker, M.G., Watson, D., Park, T., et al., 2004. A multigene assay to predict recurrence of tamoxifen-treated, node-negative breast cancer. N. Engl. J. Med. 351, 2817–2826.

Pathak, S., Meng, W.J., Zhang, H., Gnosa, S., Nandy, S.K., Adell, G., Holmlund, B., Sun, X.F., 2014. Tafazzin protein expression is associated with tumorigenesis and radiation response in rectal cancer: a study of Swedish clinical trial on preoperative radiotherapy. PloS One 9, e98317.

Pridham, K.J., Le, L., Guo, S., Varghese, R.T., Algino, S., Liang, Y., Fajardin, R., Rodgers, C.M., Simonds, G.R., Kelly, D.F., et al., 2018. PIK3CB/p110beta is a selective survival factor for glioblastoma. Neuro Oncol. 20, 494–505.

Qi, L., Chen, L., Li, Y., Qin, Y., Pan, R., Zhao, W., Gu, Y., Wang, H., Wang, R., Chen, X., et al., 2016a. Critical limitations of prognostic signatures based on risk scores summarized from gene expression levels: a case study for resected stage I non-small-cell lung cancer. Briefings Bioinf. 17, 233–242.

Qi, L., Li, Y., Qin, Y., Shi, G., Li, T., Wang, J., Chen, L., Gu, Y., Zhao, W., Guo, Z., 2016b. An individualised signature for predicting response with concordant survival benefit for lung adenocarcinoma patients receiving platinum-based chemotherapy. Br. J. Cancer 115, 1513–1519.

Quinlan, A.R., Hall, I.M., 2010. BEDTools: a flexible suite of utilities for comparing genomic features. Bioinformatics 26, 841–842.

Ricketts, C.J., De Cubas, A.A., Fan, H., Smith, C.C., Lang, M., Reznik, E., Bowlby, R., Gibb, E.A., Akbani, R., Beroukhim, R., et al., 2018. The cancer genome atlas comprehensive molecular characterization of renal cell carcinoma. Cell Rep. 23, 3698.

Sato, Y., Yoshizato, T., Shiraishi, Y., Maekawa, S., Okuno, Y., Kamura, T., Shimamura, T., Sato-Otsubo, A., Nagae, G., Suzuki, H., et al., 2013. Integrated molecular analysis of clear-cell renal cell carcinoma. Nat. Genet. 45, 860–867.

Senbabaoglu, Y., Michailidis, G., Li, J.Z., 2014. Critical limitations of consensus clustering in class discovery. Sci. Rep. 4, 6207.

Starling, R.C., Pham, M., Valantine, H., Miller, L., Eisen, H., Rodriguez, E.R., Taylor, D.O., Yamani, M.H., Kobashigawa, J., McCurry, K., et al., 2006. Molecular testing in the management of cardiac transplant recipients: initial clinical experience. J. Heart Lung Transplant. 25, 1389–1395.

Su, J., Zhang, Q., Qi, H., Wu, L., Li, Y., Yu, D., Huang, W., Chen, W.D., Wang, Y.D., 2017. The G-protein-coupled bile acid receptor Gpbar1 (TGR5) protects against renal inflammation and renal cancer cell proliferation and migration through antagonizing NF-kappaB and STAT3 signaling pathways. Oncotarget 8, 54378–54387.

Takahashi, M., Rhodes, D.R., Furge, K.A., Kanayama, H., Kagawa, S., Haab, B.B., Teh, B.T., 2001. Gene expression profiling of clear cell renal cell carcinoma: gene identification and prognostic classification. Proc. Natl. Acad. Sci. U. S. A. 98, 9754–9759.

Tatlow, P.J., Piccolo, S.R., 2016. A cloud-based workflow to quantify transcript-expression levels in public cancer compendia. Sci. Rep. 6, 39259.

Toll, L., Jimenez, L., Waleh, N., Jozwiak, K., Woo, A.Y., Xiao, R.P., Bernier, M., Wainer, I.W., 2011. {Beta}2-adrenergic receptor agonists inhibit the proliferation of 1321N1 astrocytoma cells. J. Pharmacol. Exp. Therapeut. 336, 524–532.

Tomita, K., Izumi, K., Okabe, S., 2003. Roxatidine- and cimetidine-induced angiogenesis inhibition suppresses growth of colon cancer implants in syngeneic mice. J. Pharmacol. Sci. 93, 321–330.

Turanli, B., Altay, O., Boren, J., Turkez, H., Nielsen, J., Uhlen, M., Arga, K.Y., Mardinoglu, A., 2019a. Systems biology based drug repositioning for development of cancer therapy. Semin. Canc. Biol.

Turanli, B., Karagoz, K., Gulfidan, G., Sinha, R., Mardinoglu, A., Arga, K.Y., 2018. A network-based cancer drug discovery: from integrated multi-omics approaches to precision medicine. Curr. Pharmaceut. Des. 24, 3778–3790.

Turanli, B., Zhang, C., Kim, W., Benfeitas, R., Uhlen, M., Arga, K.Y., Mardinoglu, A., 2019b. Discovery of therapeutic agents for prostate cancer using genome-scale metabolic modeling and drug repositioning. EBioMed. 42, 386–396.

Uhlen, M., Zhang, C., Lee, S., Sjostedt, E., Fagerberg, L., Bidkhori, G., Benfeitas, R., Arif, M., Liu, Z., Edfors, F., et al., 2017. A pathology atlas of the human cancer transcriptome. Science 357.

Wang, H., Zhang, H., Dai, Z., Chen, M.S., Yuan, Z., 2013. TSG: a new algorithm for binary and multi-class cancer classification and informative genes selection. BMC Med. Genom. 6 (Suppl 1), S3.

Wilkerson, M.D., Hayes, D.N., 2010. ConsensusClusterPlus: a class discovery tool with confidence assessments and item tracking. Bioinformatics 26, 1572–1573.

Winslow, R.L., Trayanova, N., Geman, D., Miller, M.I., 2012. Computational medicine: translating models to clinical care. Sci. Transl. Med. 4, 158rv111.

Wishart, D.S., Knox, C., Guo, A.C., Shrivastava, S., Hassanali, M., Stothard, P., Chang, Z., Woolsey, J., 2006. DrugBank: a comprehensive resource for in silico drug discovery and exploration. Nucleic Acids Res. 34, D668–672.

Xia, M., Liu, J., Liu, S., Chen, K., Lin, H., Jiang, M., Xu, X., Xue, Y., Liu, W., Gu, Y., et al., 2017. Ash1l and lnc-Smad3 coordinate Smad3 locus accessibility to modulate iTreg polarization and T cell autoimmunity. Nat. Commun. 8, 15818.

Xie, R., Chen, X., Chen, Z., Huang, M., Dong, W., Gu, P., Zhang, J., Zhou, Q., Dong, W., Han, J., et al., 2019. Polypyrimidine tract binding protein 1 promotes lymphatic metastasis and proliferation of bladder cancer via alternative splicing of MEIS2 and PKM. Cancer Lett. 449, 31–44.

Yan, H.X., Zhang, Y.J., Zhang, Y., Ren, X., Shen, Y.F., Cheng, M.B., Zhang, Y., 2017. CRIF1 enhances p53 activity via the chromatin remodeler SNF5 in the HCT116 colon cancer cell lines. Biochim. Biophys. Acta Gene Regul. Mech. 1860, 516–522.

Yang, J.Q., Liu, H., Diaz-Meco, M.T., Moscat, J., 2010. NBR1 is a new PB1 signalling adapter in Th2 differentiation and allergic airway inflammation in vivo. EMBO J. 29, 3421–3433.

Yang, P., Li, Z., Fu, R., Wu, H., Li, Z., 2014. Pyruvate kinase M2 facilitates colon cancer cell migration via the modulation of STAT3 signalling. Cell. Signal. 26, 1853–1862.

Yang, W., Xia, Y., Hawke, D., Li, X., Liang, J., Xing, D., Aldape, K., Hunter, T., Alfred Yung, W.K., Lu, Z., 2012. PKM2 phosphorylates histone H3 and promotes gene transcription and tumorigenesis. Cell 150, 685–696.

Yang, W., Xia, Y., Ji, H., Zheng, Y., Liang, J., Huang, W., Gao, X., Aldape, K., Lu, Z., 2011. Nuclear PKM2 regulates beta-catenin transactivation upon EGFR activation. Nature 480, 118–122.

Yu, G., Wang, L.G., Han, Y., He, Q.Y., 2012. clusterProfiler: an R package for comparing biological themes among gene clusters. OMICS 16, 284–287.

Yuan, F., Zhang, Y., Ma, L., Cheng, Q., Li, G., Tong, T., 2017. Enhanced NOLC1 promotes cell senescence and represses hepatocellular carcinoma cell proliferation by disturbing the organization of nucleolus. Aging Cell 16, 726–737.

Zhao, H., Ljungberg, B., Grankvist, K., Rasmuson, T., Tibshirani, R., Brooks, J.D., 2006. Gene expression profiling predicts survival in conventional renal cell carcinoma. PLoS Med. 3, e13.